

Supporting Information

Exploring Carbon Electrode Parameters in Li-O₂ Cells: Li₂O₂ and Li₂CO₃ Formation

Bianca P. Sousa^a, Chayene G. Anchieta^b, Thayane M. C. Nepel^a, Alex R. Neale^c, Laurence J. Hardwick^c, Rubens M. Filho^a, Gustavo Doubek^{a*}

a: Laboratory of Advanced Batteries, School of Chemical Engineering, University of Campinas (UNICAMP), 500, Avenida Albert Einstein, 13083-852, Campinas, São Paulo, Brazil.

b: Swiss Light Source, Paul Scherrer Institut, Forschungsstrasse 111, 5232 Villigen, Switzerland

c: Stephenson Institute for Renewable Energy, Department of Chemistry, Peach Street, University of Liverpool, Liverpool L69 7ZF, United Kingdom.

* Corresponding author. E-mail: doubek@unicamp.br

Figures S1 present images of the cell used for electrochemical tests with limited capacity of $650 \mu\text{Ah}\cdot\text{cm}^{-2}$. It consists in a commercial E1-Cell basis and a custom-made stainless steel lid with channels for O_2 flow and glass window.

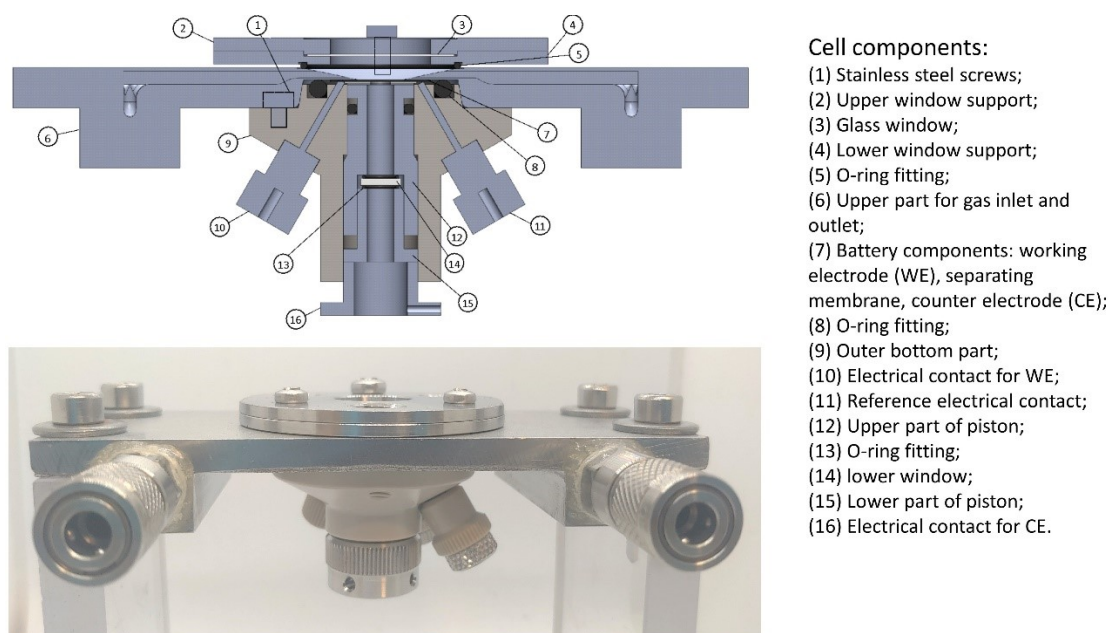


Figure S1. Scheme and digital images of the cell used for operando Raman tests, with all components indicated. [1]

Similarly, Figure S2 shows images of the home-made cell used for deep discharge/charge tests with Swagelok-type system for gas flow.

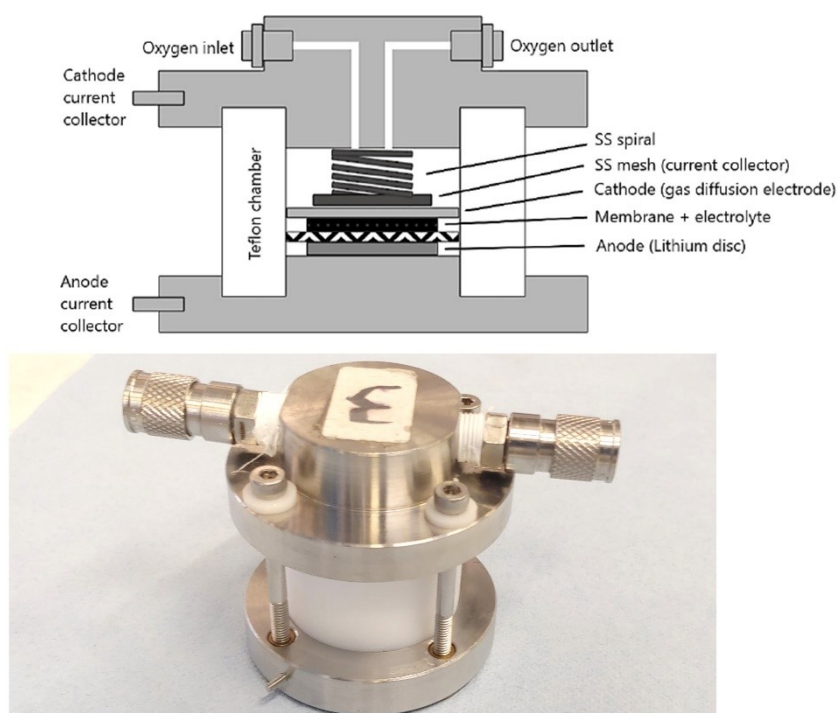


Figure S2. Scheme and digital image of the cell used for electrochemical deep discharge/charge test with all components indicated.[2]

The Raman bands observed in the spectra presented in Figures 2, 3 and 5 of the main text are described in Table S1 with their respective assignment and reference.

Table S1. Raman bands assignment related to the spectra presented in Figures 1, 2 and 5.

Species	Wavenumber (cm ⁻¹)	Assignment	References
Li ₂ O ₂	790	O-O stretch	[3], [4], [5]
Li ₂ CO ₃	1090	C-O stretch	[3], [6], [7]
LiO ₂	1130	O-O stretch	[3], [4]
Carbon (CNT, CP)	1200	D* band - Related to functional groups	[8], [9], [10], [11]
	1330	D band - Related to structural defects	
	1500	D'' band - Related to amorphous carbon	
	1584	G band - From E _{g2} mode	
	1615	D' band - Related to structural defects	
LiClO ₄	931	Cl-O stretch	[12],[13], [14]
DMSO (dimethyl sulphoxide)	953	CH ₃ rocking	[15], [12], [3]
	1026	SO symmetric stretch of dimer	
	1042	SO antisym. stretch of dimer	
	1058	SO symm. stretch of monomer	
	1420	CH ₃ asymmetric deformation	
DMSO ₂ (dimethyl sulphoxone)	498	SO ₂ deformation	[16]
	698	CS ₂ symmetric stretch	
	1004	CH ₃ rock	
	1128	SO ₂ symmetric stretch	
	1428	CH ₃ deformation	

Information of the different carbon nanotubes used in this work are presented in Table S2 and Figure S3. Table S2 show the physical characteristics and the manufacturer of the CNTs, while Figure S3 present XPS and Raman spectra of the electrodes with CNTs.

Table S2. Characteristics of different CNTs used.

	Manufacturer	Outside diameter (nm)	Length (μm)	Carbon content (%)
CNT_SA	Sigma-Aldrich	7 - 15	0.5 - 10	> 99
CNT_CCL	CNT Co., Ltd.	10 - 40	1 - 25	> 95

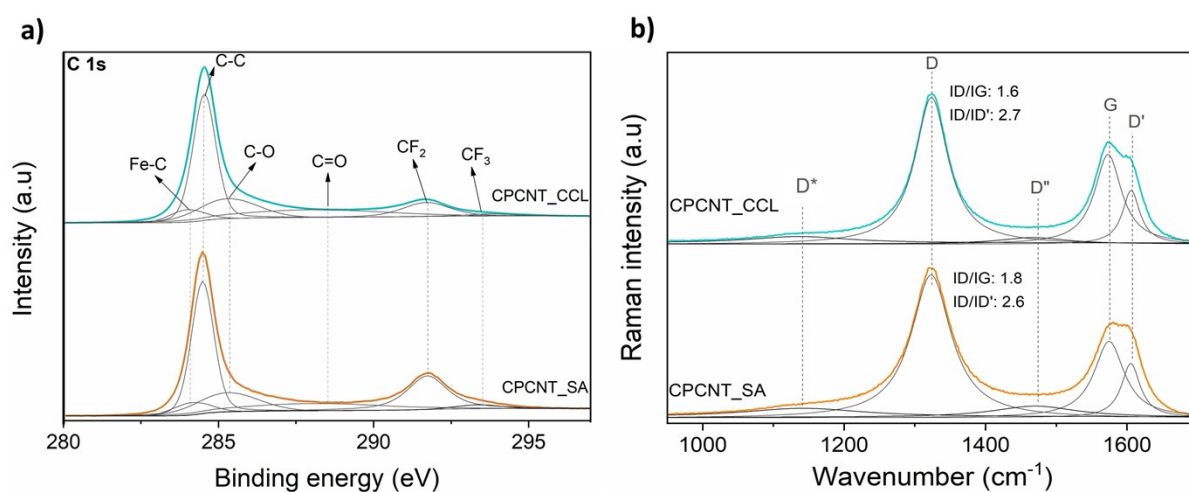


Figure S3. a) XPS and b) Raman spectra of pristine CPCNT_SA and CPCNT_CCL electrodes.

XPS show that both electrodes present C-C, C-O, C=O, CF₂, CF₃, and Fe-Ce bonding. Raman spectra of the CNTs contains D, G, D', D* and D'' bands. Electrode CPCNT_SA present higher CF bonds in XPS and higher I_D/I_G ratio, indicating more structural defects.

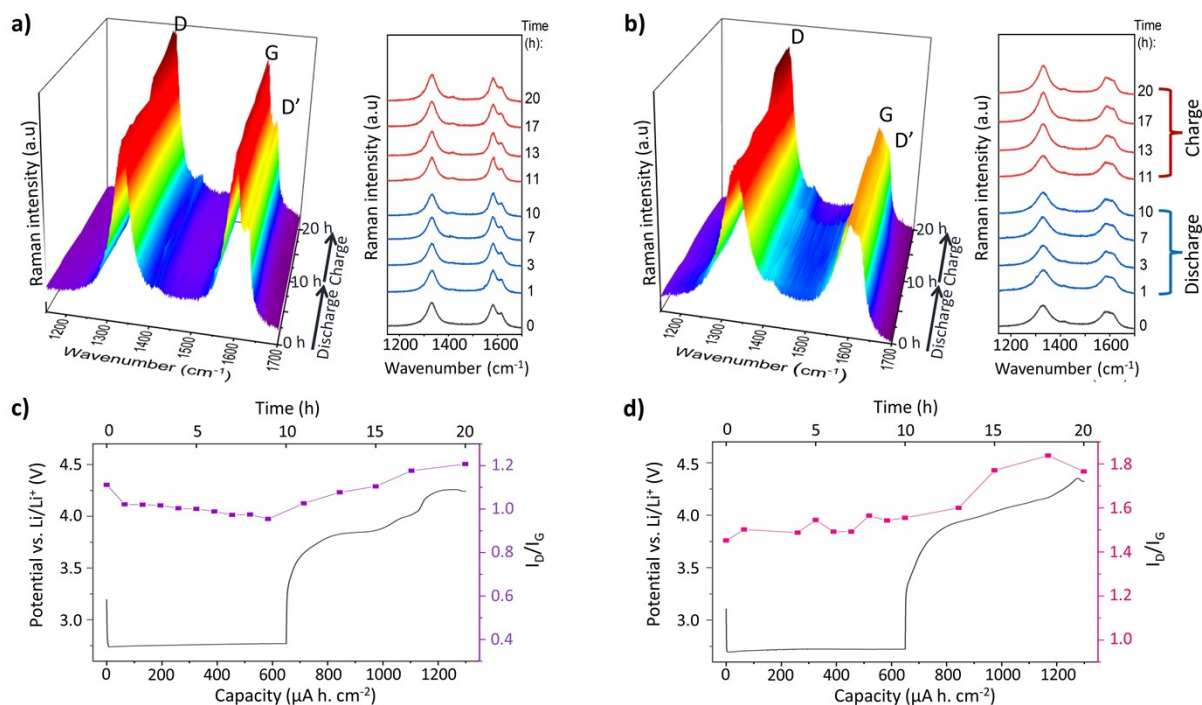


Figure S4. Operando Raman spectra in carbon range, and I_D/I_G ratio graph of carbon bands with electrochemical discharge/charge profile of electrodes a,c) Carbon paper with CNT from CNT Co. Ltd. and Nafion binder, and b,d) Carbon paper with CNT from Sigma-Aldrich and PTFE binder in a Li-O₂ cell with 0.1 M DMSO/LiClO₄ electrolyte at current density $j= 65 \mu\text{A cm}^{-2}$.

The Raman spectra with elapsed time in the carbon region and I_D/I_G with electrochemical profile of the electrodes with different CNTs and binders has the same behaviour of the electrode with CNT presented in Figure 3 of the main text. D band increase upon charging indicating occurrence of side reactions in the carbon surface.

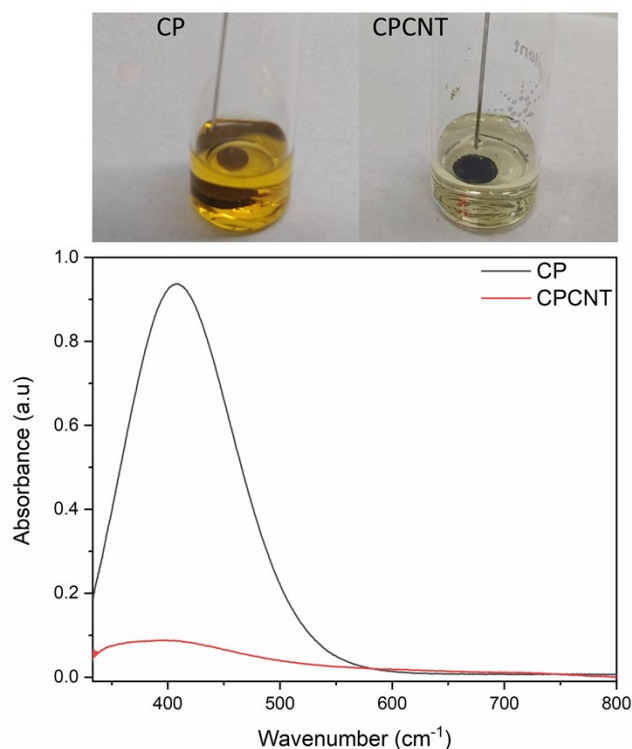


Figure S5. Digital image of discharged carbon paper (CP) and CP with CNT electrodes at 650 uAh cm^{-2} in TiOSO_4 solution and their respective UV-Vis spectra.

The TiOSO_4 solution with CP electrode becomes bright yellow and has a strong absorbance at $\lambda = 406 \text{ nm}$, indicating great amount of Li_2O_2 . In the opposite, CP with CNT promotes a light change in the solution colour, which present a weak absorbance in the UV-Vis spectra, indicating small amount of Li_2O_2 . The results in Figure S5 confirms the difference in the main discharge product of the electrodes, which are Li_2O_2 for CP and Li_2CO_3 for CP with CNT electrodes.

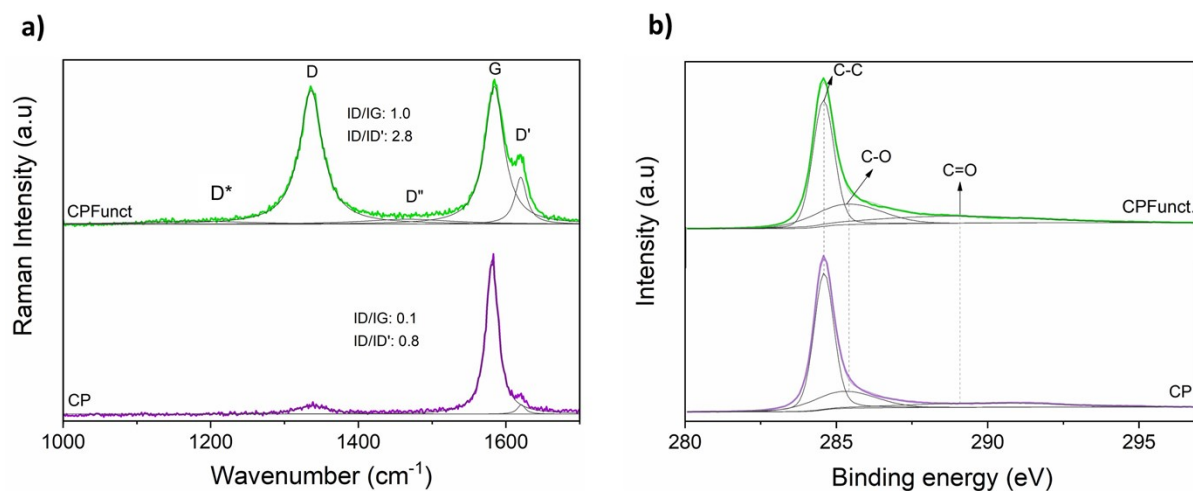


Figure S6. (a) Raman and (b) XPS spectra of pristine carbon paper and carbon paper after O_2 plasma functionalization.

Raman in Figure S6a show that CP submitted to O₂ plasma for functionalization present D* and D'' carbon bands, and higher D band when compared with pure CP, indicating more defects. XPS spectrum of CP functionalized present higher peaks of CO bonds than the pristine CP. These spectra confirms that the procedure with O₂ plasma successfully induced structural defects and CO bonds in the carbon paper.

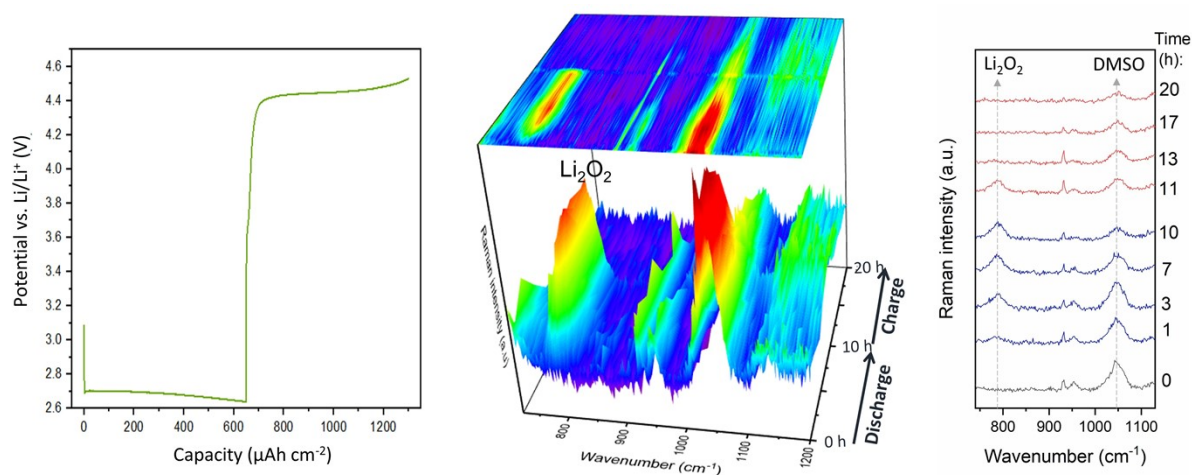


Figure S7. Operando Raman of carbon paper functionalized electrode in battery using 0.1M DMSO/LiClO₄ electrolyte and applied current density of 65 $\mu\text{A cm}^{-2}$.

Raman spectra with elapsed time of the CP functionalized in Li-O₂ battery with DMSO/LiClO₄ electrolyte show Li₂O₂ forming on discharging and decomposing on charging. Bands assigned to DMSO decrease during the cycle due to a focus issue in the measurement. No band related to lithium carbonate is detected.

The areas of XPS peaks presented in Figure 4 in the main paper are shown in percentage in Table S3. The table shows photoemission data of Fe 2p, C 1s, and F 1s of electrodes carbon paper with CNT (CPCNT) pristine and after discharge.

Table S3. Percentage areas of XPS peaks of iron, carbon and fluorine bindings in CPCNT pristine and discharged electrodes.

Photoemission	Binding	Binding energy (eV)	Percentage area	
			Pristine	Discharged
Fe 2p	Fe ²⁺	711.0	11.2	15.9
	Fe ³⁺	714.0	25.7	23.6
	Fe ²⁺	724.0	2.7	3.4
	Fe ³⁺	727.0	0.9	0.9
	Fe-C	707.0	27.3	26.7
	Fe-C	720.0	22.3	21.9
C 1s	C-Fe	284.1	5.7	4.5
	C-C	284.5	41.2	42.0
	C-O	285.3	14.8	18.3
	C=O	288.0	13.7	13.9
	CF ₂	291.9	22.5	19.9
	CF ₃	293.8	2.1	1.3
F 1s	CF ₂	689.0	96.6	91.8
	CF ₃	690.8	3.4	3.5
	Fe-F	685.4	-	4.7

XPS in carbon energy of CP electrode pristine and after discharge were also carried out and shown in Figure S8 with the relative percentage area of XPS peaks. Compared to CP pristine, a slight decrease in C-C bond and increase in C-O bond are observed in the CP discharged. These changes are probably related to the presence of Li_2O_2 on the discharged CP surface and its higher interaction with oxygen from the product.

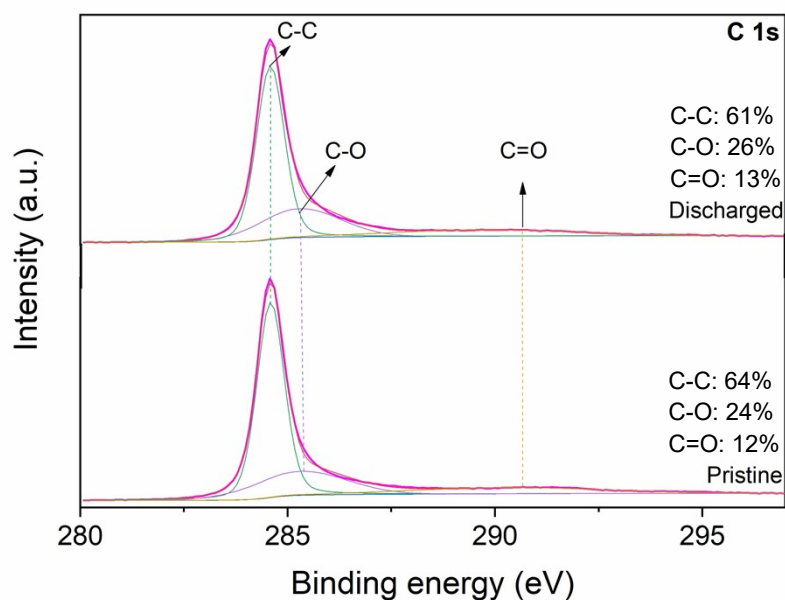


Figure S8. XPS spectra in C 1s energy of carbon paper electrode pristine and discharged.

References:

- [1] Intellectual Property/Patent: Hermetic device allows different electrochemical characterization techniques for Metal-Air batteries. UNICAMP. BR 10 2020 026298. 21.
- [2] B. A. B. FRANCISCO. Avaliação das Condições de Operação e da Influência de Eletrólito em Baterias Lítio-Oxigênio. Dissertation. Campinas: Universidade Estadual de Campinas, 2020.
- [3] GITTLESON, F. S. et al. Raman Spectroscopy in Lithium-Oxygen Battery Systems. **Chem electrochem**, v. 2, n. 10, p.1446-1457, 2015.
- [4] PENG, Zhangquan et al. Oxygen Reactions in a Non-Aqueous Li^+ Electrolyte. **Angewandte Chemie International Edition**, v. 50, n. 28, p.6351-6355, 2011.
- [5] YANG, Junbing et al. Evidence for lithium superoxide-like species in the discharge product of a $\text{Li}-\text{O}_2$ battery. **Physical Chemistry Chemical Physics**, v. 15, n. 11, p.3764-3771, 2013.
- [6] BROOKER, M. H.; BATES, J. B. Raman and Infrared Spectral Studies of Anhydrous Li_2CO_3 and Na_2CO_3 . **The Journal of chemical physics**, v. 54, n.11, p. 4788-4796, 1971.

- [7] QIAO, Y. et al. Li-CO₂ Electrochemistry: A New Strategy for CO₂ Fixation and Energy Storage. **Joule**, v. 1, p. 1-12, 2017.
- [8] DETTLAFF, Anna et al. High-performance method of carbon nanotubes modification by microwave plasma for thin composite films preparation. **Rsc Advances**, v. 7, n. 51, p.31940-31949, 2017.
- [9] DRESSELHAUS, M.s. et al. Raman spectroscopy of carbon nanotubes. **Physics Reports**, v. 409, n. 2, p.47-99, mar. 2005.
- [10] FERRARI, Andrea C.; BASKO, Denis M.. Raman spectroscopy as a versatile tool for studying the properties of graphene. **Nature Nanotechnology**, v. 8, n. 4, p.235-246, abr. 2013.
- [11] NUNES, Willian G. et al. Surface and Electrochemical Properties of Radially Oriented Multiwalled Carbon Nanotubes Grown on Stainless Steel Mesh. *Journal Of The Electrochemical Society*, [s.l.], v. 165, n. 16, p.3684-3696, 2018.
- [12] WANG, Zhaoxiang et al. Vibrational spectroscopic study of the interaction between lithium perchlorate and dimethylsulfoxide. **Electrochimica Acta**, v. 42, n. 17, p.2611-2617, 1997.
- [13] XUAN, X, et al. A VIBRATIONAL SPECTROSCOPIC STUDY OF ION SOLVATION IN LITHIUM PERCHLORATE/PROPYLENE CARBONATE ELECTROLYTE. *Phys. Ch. Uq.*, 2001, Vol. 39, pp. 327-342, 2001.
- [14] COSTA, L T. et al. Raman spectra of polymer electrolytes based on poly(ethylene glycol)dimethyl ether, lithium perchlorate, and the ionic liquid 1-butyl-3-methylimidazolium hexafluorophosphate. *Vibrational Spectroscopy* v. 54, p. 155–158, 2010.
- [15] MARTENS, W. N. et al. Raman spectroscopy of dimethyl sulphoxide and deuterated dimethyl sulphoxide at 298 and 77 K. **J. Raman Spectrosc**, v. 33, p. 84-91, 2002.
- [16] MCLACHLAN, R.d.; CARTER, V. Vibrational spectra of crystalline dimethyl sulfone. **Spectrochimica Acta Part A: Molecular Spectroscopy**, v. 26, n. 5, p.1121-1127,1970.